

PAPER

Ultrafast, miniature soft actuators

To cite this article: Onur Bas *et al* 2021 *Multifunct. Mater.* 4 045001

View the [article online](#) for updates and enhancements.

You may also like

- [First-principles DFT investigations of the vibrational spectra of chloro-quine and hydroxychloroquine](#)
Xiao-Yan Liu, Ya-Ning Xu, Hao-Cheng Wang *et al.*
- [Single-beam multimodal nonlinear-optical imaging of structurally complex events in cell-cycle dynamics](#)
A A Lanin, A S Chebotarev, I V Kelmanson *et al.*
- [Demonstrating the first postulate of relativity in a lift](#)
Stephen Hughes and Tim Croxford



The Electrochemical Society
Advancing solid state & electrochemical science & technology

241st ECS Meeting

May 29 – June 2, 2022 Vancouver • BC • Canada

Extended abstract submission deadline: Dec 17, 2021

Connect. Engage. Champion. Empower. Accelerate.
Move science forward



Submit your abstract



Multifunctional Materials



PAPER

Ultrafast, miniature soft actuators

RECEIVED
21 June 2021

REVISED
30 September 2021

ACCEPTED FOR PUBLICATION
13 October 2021

PUBLISHED
1 November 2021

Onur Bas^{1,2,*} , Benjamin Gorissen³ , Simon Luposchinsky^{2,4}, Tara Shabab² , Katia Bertoldi³ 
and Dietmar W Hutmacher^{1,2,*} 

¹ ARC Industrial Transformation Training Centre in Additive Biomanufacturing, Queensland University of Technology (QUT), Brisbane, QLD 4059, Australia

² School of Mechanical, Medical and Process Engineering, Queensland University of Technology (QUT), Brisbane, QLD 4001, Australia

³ Harvard John A. Paulson School of Engineering and Applied Sciences, Harvard University, Cambridge, MA 02138, United States of America

⁴ Department of Functional Materials in Medicine and Dentistry, University of Würzburg, Pleicherwall 2, Würzburg 97070, Germany

* Authors to whom any correspondence should be addressed.

E-mail: o.bas@qut.edu.au and dietmar.hutmacher@qut.edu.au

Keywords: soft robotics, actuators, composites, fibers, inflatable, fast

Supplementary material for this article is available [online](#)

Abstract

The quest for an advanced soft robotic actuator technology that is fast and can execute a wide range of application-specific tasks at multiple length scales is still ongoing. Here, we demonstrate a new design and manufacturing strategy that leads to high-speed inflatable actuators exhibiting diverse movements. Our approach leverages the concept of miniaturisation to reduce the required volume of fluid for actuation as well as fibre-reinforcement to improve the efficiency of actuators in converting delivered fluids into fast and predictable movement. To fabricate the designs, we employ a class of additive manufacturing technology called melt electrowriting. We demonstrate 3D printing of microfibre architectures on soft elastomers with precision at unprecedentedly small length scales, leading to miniaturised composite actuators with highly controlled deformation characteristics. We show that owing to their small dimensions and deterministically designed fibrous networks, our actuators require extremely low amounts of fluid to inflate. We demonstrate that actuators with a length of 10–15 mm and an inner diameter 1 mm can reach their full range of motion within ~ 20 ms without exploiting snapping instabilities or material non-linearities. We display the speed of our actuators by building an ultrafast, soft flycatcher. We also show that our actuators outperform their counterparts with respect to achievable movement diversity and complexity.

1. Introduction

The field of soft robotics proposed the development of versatile actuators as one of the first marks on its roadmap to next-generation robotics, due to the integral role of these technologies in the function and performance of robots [1–3]. It is known that actuators determine the size, cost, power source, control mechanism, and general design of any robotic system [4], therefore strong emphasis has been placed on the advancement of these components. Although a wide range of actuator designs have been proposed, due to their ease of operation, low cost and ability to achieve a large range of deformations, inflatable actuators have been the primary subject of interest [5]. However, these actuators are often considered too slow for most applications as their speed is limited by large inflation volumes that are needed to create deformations and the consequent large viscous forces needed to let this volume pass through narrow tubes. Several design strategies leveraging snapping instabilities [6], material non-linearity [7], stored elastic energy [8], as well as explosive chemical reactions [9] have been proposed to overcome this limitation. However, the functionality of the resulting inflatable actuators is highly limited as very specific considerations have to be taken into account in their design and manufacturing. Combining high actuation speeds without compromising functionality has been a major challenge and a high-speed inflatable actuator concept that can execute an

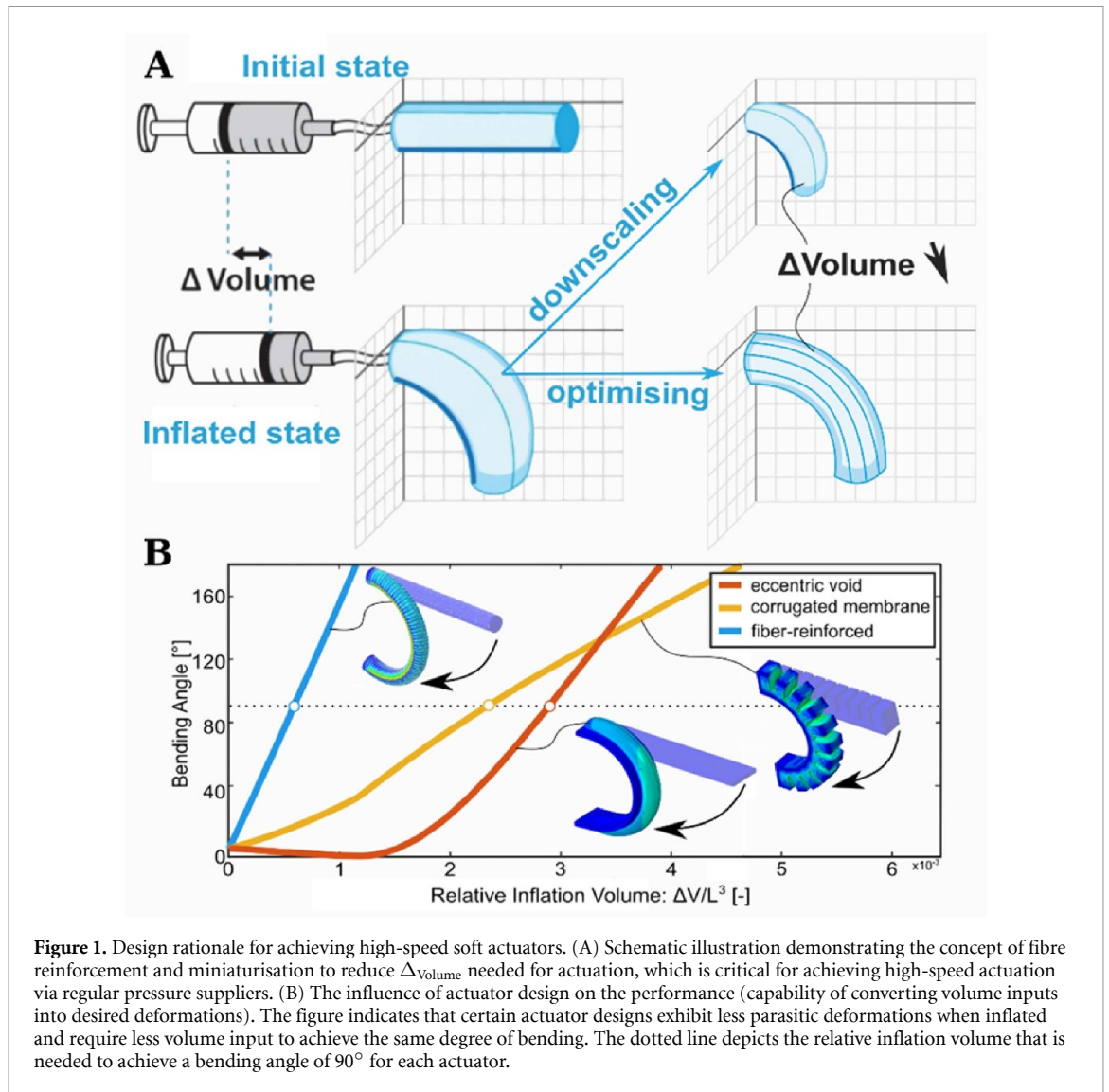
extensive range of application-specific tasks is yet to be demonstrated. In this work, we aim at developing highly functional and modular actuators that achieve high speeds.

2. Results and discussions

To accomplish this goal, we investigate mechanisms that lay at the basis of nature's fast-acting structures that rely on the transportation of fluids for actuation. It has been shown that these fluid-driven actuators harness miniaturisation to achieve fast movements [10]. For instance, the Aldrovanda can close its leaves in 20 ms, which is ~ 10 times more rapidly than the Venus flytrap, due to its significantly smaller size (approximately 1/10th of Venus flytrap) [10]. Miniaturised designs influence both the required volume of fluid (ΔV_{volume}) that is needed to be displaced, as well as the distance it needs to travel, enabling rapid movements. Thus, we hypothesise that an analogous miniaturisation strategy can be applied to inflatable actuators (see figure 1(A) for the schematic illustration of the concept).

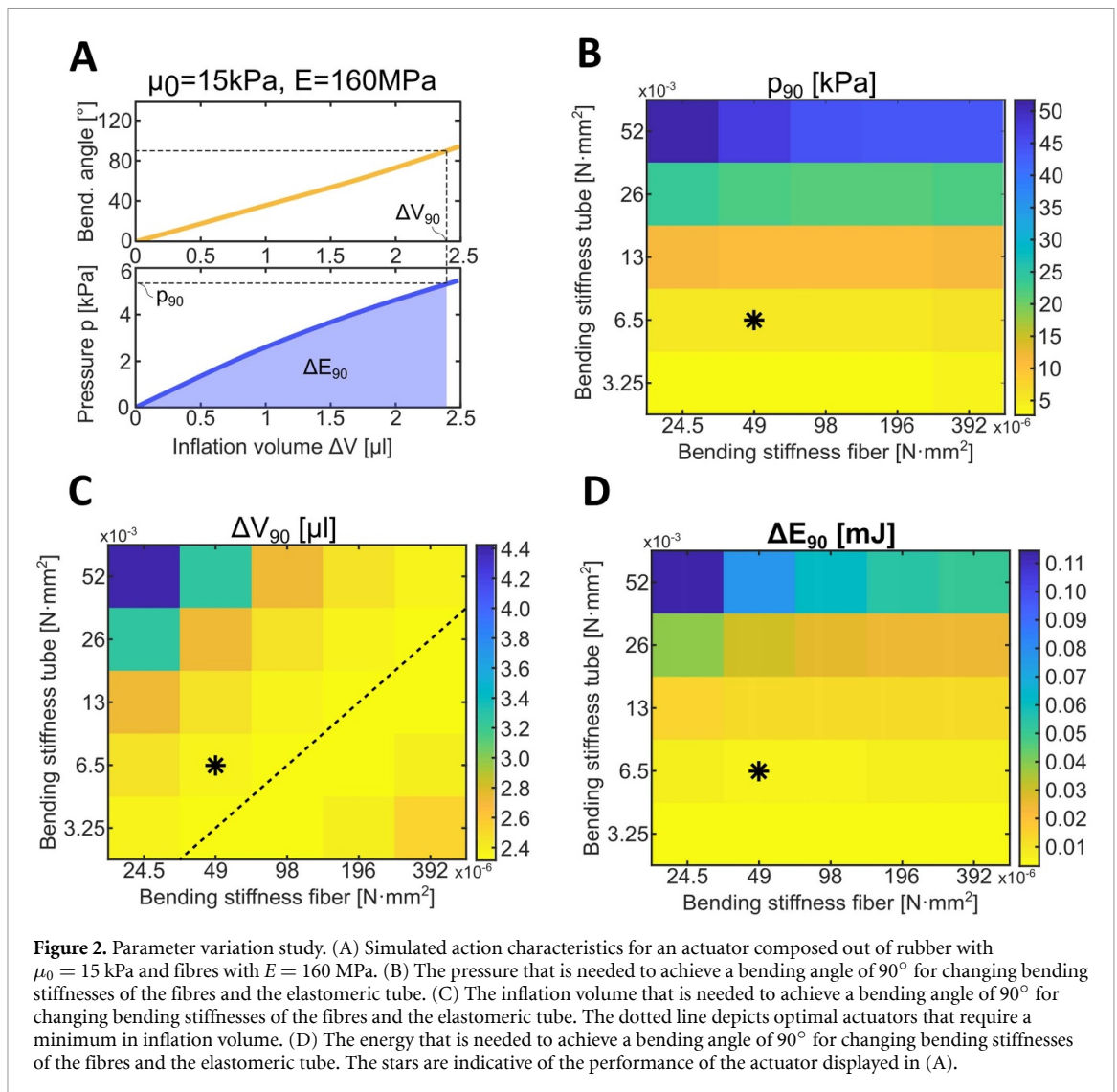
In addition to miniaturisation, it is essential to improve the efficiency of actuators in converting delivered fluids into fast and predictable movement. As the transportation of fluids is a challenge in these systems, available volume influx has to be efficiently converted towards desired deformations by avoiding unnecessary volumetric expansions that do not contribute to the overall desired deformation (figure 1(A)). To determine how design can influence this efficiency, we performed finite element (FE) simulations (see supplementary text for further information available online at stacks.iop.org/MFM/4/045001/mmedia) on three common bending actuator designs (eccentric [11], corrugated membrane [12] and fibre-reinforced [13]) and measured the inflation volume required to obtain the same degree of bending. To eliminate the effect of size, we normalised the inflation volume by L^3 , where we have taken the length 'L' of the actuator as the characteristic length scale. From this analysis, we verify that the design of actuators has a major influence on bending performance. The same bending angle is reached at lower input volume for those designs that limit parasitic expansion and cross-sectional deformations. As shown in figure 1(B), the actuator with an eccentric design [14] first has to be inflated substantially to start bending. Then, more than 5 times ΔV_{volume} has to be delivered to achieve 90° bending when compared to the fibre-reinforced actuator design. Similarly, the formation of major bulges can be seen in the corrugated membrane actuator design, which is the hallmark of compromised performance. Based on these findings, we conclude that deterministically designed high-modulus fibre architectures are effective in converting fluid volume influx into the desired deformation. In addition to their efficiency, which is largely overlooked and yet to be exploited in the literature, fibre-reinforced actuators are proven to be highly versatile with their ability to achieve tailored motions [13, 15], making them the ideal choice in our application.

While the previous analysis pointed that fibre reinforced design has the highest potential to achieve high speeds, it did not provide any information regarding the influence of the materials and/or geometry on the performance of the actuators. To investigate the dependency of inflation volume on these two factors, we conducted a series of FE analyses. We designed and simulated a fibre reinforced bending actuator consisting of double-helical fibres (both clockwise and counterclockwise) with a pitch of $390 \mu\text{m}$ as well as three longitudinally placed fibres on one side that create bending, surrounding a hollow cylinder with an internal diameter of 1 mm, a wall thickness of 0.2 mm and length of 10 mm. In our simulations (which were conducted using the commercial code Abaqus/Standard), we discretised the cylinder using second-order hybrid tetrahedral elements (element type: C3D10H and the fibres with three-node quadratic beam elements (element type: B32) and actuated the models supplying incompressible fluid to the internal cavity via a fluid-cavity interaction. We modelled the material of the cylinder as incompressible neo-Hookean with the initial shear modulus μ_0 , while the fibres are assumed to be linear elastic with Young's modulus E and Poisson's ratio of 0.3. To begin with, we considered $\mu_0 = 15 \text{ kPa}$ and $E = 160 \text{ MPa}$ and found that both the bending angle and pressure vary more or less linear with inflation volume (see figure 2). From the graphs of figure 2(A), we can identify three actuator characteristics: the inflation volume that is needed to achieve a bending angle of 90° (ΔV_{90}), the corresponding pressure (p_{90}) and the needed energy (ΔE_{90}), which can be calculated as the area under the pressure–volume curve. For this particular actuator, $\Delta V_{90} = 2.35 \mu\text{l}$, $p_{90} = 5.4 \text{ kPa}$ and $\Delta E_{90} = 0.0064 \text{ mJ}$. Next, we tested different initial shear moduli values ranging between $7.5 \text{ kPa} < \mu_0 < 120 \text{ kPa}$ for the elastomeric matrix and Young's moduli values ranging between $80 \text{ Mpa} < E < 1.28 \text{ Gpa}$ for the fibres. As these two parameters directly influence the bending stiffness of either the cylinder ($EI = 3\mu_0 \times \pi/4 \cdot (r_o^4 - r_i^4)$, with r_o and r_i being the inner and outer radius of the cylinder) and the fibres ($EI = E \times \pi/4 \times r^4$, with r being the fibre radius), we can use them to assess the influence of both geometrical and material parameters on the performance of the actuators. In figures 2(B)–(D), we display these influences by plotting respectively ΔV_{90} , p_{90} and ΔE_{90} for different bending stiffnesses of both the cylinder or the surrounding fibres, where stars indicate the previously reported values. Regarding the pressure that is needed to achieve a 90° bending angle (figure 2(B)), we can



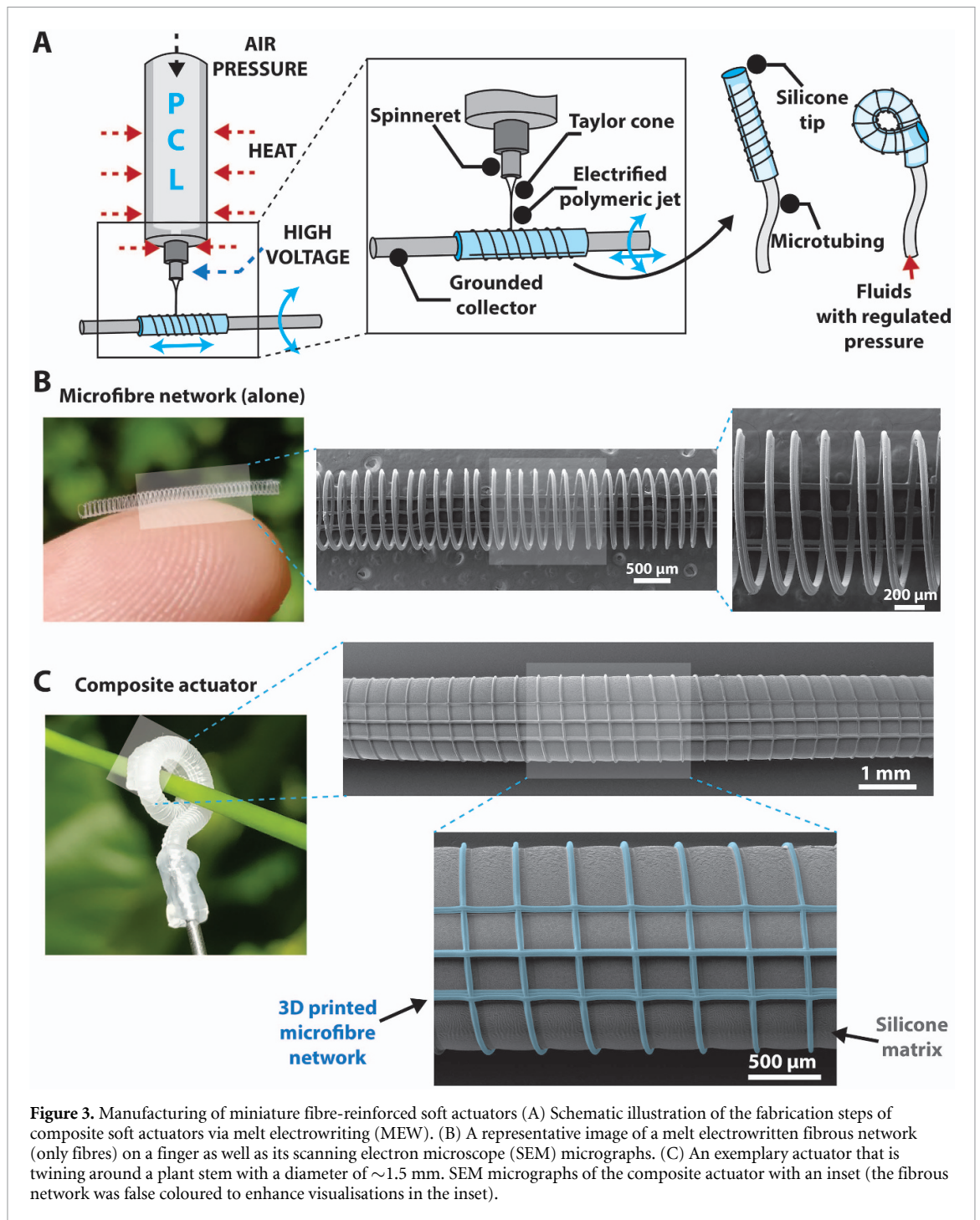
conclude that a higher pressure is needed when the bending stiffness of the cylinder increases. Surprisingly, the bending stiffness of the fibre does not have a large influence on the required input pressure levels. Regarding the inflation volume (figure 2(C)), we found that a combination of a stiff tube with compliant fibres and a combination of stiff fibres with a compliant tube lead to higher inflation volumes than when both are stiff or compliant. We can thus conclude that there is an optimal ratio of bending stiffnesses, where fibres need to be ~ 15 times stiffer than the elastomeric matrix, which has been indicated by a dotted line on the figure. Lastly, The energy that is needed to bend 90° (figure 2(D)) is dominated by and follows the same trends as the pressure dependency, which is logical since the relative pressure variation is larger than the relative volume variation while varying stiffnesses.

To create these highly dynamic bending actuators with an optimal fibre composition, we cannot rely on production processes described in the literature, as they either are incompatible with small scale production processes [13, 15–17], or lack control over fibre placements [18–20]. Therefore we developed a new manufacturing strategy that facilitates the fabrication of miniaturised composite soft actuators with precision at small length scales. We use melt electrowriting (MEW) technology [21, 22], a class of additive manufacturing system, which combines the capability of electrospinning systems to produce ultra-fine fibres (fibre diameters between 1 and $50 \mu\text{m}$) with the design freedom of 3D printing. In this automated process, we apply a thin layer of uncured soft silicone-based elastomer on the rotational collector of our MEW system. By using a rod integrated into our MEW device, we move the stage in x -direction back and forwards with an elastomer and create a thin, uniform layer of the silicone-based tubular structure. We then start MEW of fibrous network designs on this partially-cured silicone tube to achieve enhanced bonding between the fibres and matrix material (see figure 3 and movie S1 for the schematic illustration and video of the fabrication process, respectively). After the completion of the 3D printing process, we allow the silicone to fully cure and connect the actuators to a pressure source after sealing their tip.



As demonstrated in figure 4, we successfully fabricated a miniaturised bending actuator with an internal void diameter of 1 mm, length of 10 mm and a wall thickness of 0.2 mm using our manufacturing technique (see figure S1 for the technical drawing). The scanning electron micrograph (figure 4(A)) shows the accurate placement of the fibres as well as their good continuity and consistency (see table S1 for the detailed characterisation of the dimensions of the fabricated actuator). We selected the constituent materials of this actuator in accordance with the established principles depicted in figure 2. As our findings indicate that the use of soft matrix materials reduces the required actuation energy, we applied the softest grade silicone within the product family of a widely used elastomer (Ecoflex with a shore hardness of 00–10). For the fabrication of the fibre phase, we preferred polycaprolactone due to its excellent rheological properties and processability via MEW process as well as the favourable mechanical properties (elastic modulus of 320 MPa), leading to an actuator with a fibre-to-matrix bending stiffness ratio of ~ 7.5 . Although this ratio is smaller than the identified ideal ratio, our simulations suggest that this actuator (internal diameter of 1 mm, and length of 10 mm) require ΔV_{volume} of $2.3559 \mu\text{l}$ to achieve 90° bending, which is marginally higher than that of an actuator built with materials having a bending stiffness ratio of 15 (ΔV_{volume} of $2.3143 \mu\text{l}$). Overall, this material combination yielded high performant bending actuators that are also easy to manufacture, handle and characterise as demonstrated in figure 4.

After pressurizing the actuator, we indeed observed the intended large bending movements with minimum parasitic deformations (see figure 4(A)) (see figure S5 for a bending actuator without helical fibres exhibiting large parasitic deformations). Figure 4(B) shows the magnitude of the deformations achieved by the actuator at given air pressure both experimentally and as computed by means of FE modelling (see movie S2). By downscaling the dimensions to a diameter of 1 mm, we were able to fabricate bending actuators that reach full stroke (270°) when inputting only volumes of less than $7.5 \mu\text{l}$. Furthermore, by modelling the



volumetric expansion of our actuator using finite element modelling (FEM), we see radially restricted actuators are characterised by a linear displacement–volume relationship. This means that the input volume is efficiently redirected towards only one spatial dimension, giving a leveraging effect for fast actuation. To confirm this, we have tested our bending actuators under a high-frequency pneumatic input (on-off), where the input air pressure was adjusted such that a full stroke was reached at the end of the cycle (see figures 4(C) and figure S7 for details). We were able to achieve an actuation frequency reaching 30 Hz, where complete bending and recovery to the initial state takes place within ~ 30 ms (see movie S7). Further, we see that the dynamics are limited by the deflation part of the cycle. In contrast to inflation where we can adjust the input pressure to reach full stroke quicker, the deflation of the actuator is limited by an atmospheric back-pressure, resulting in a maximum actuation frequency of 30 Hz.

The presented methodology of combining miniaturisation with a fibre reinforcement design showed to be a highly successful pathway of creating highly dynamic actuators. However, this methodology is not limited to only bending deformations. Using the fabrication freedom of additive manufacturing, we can

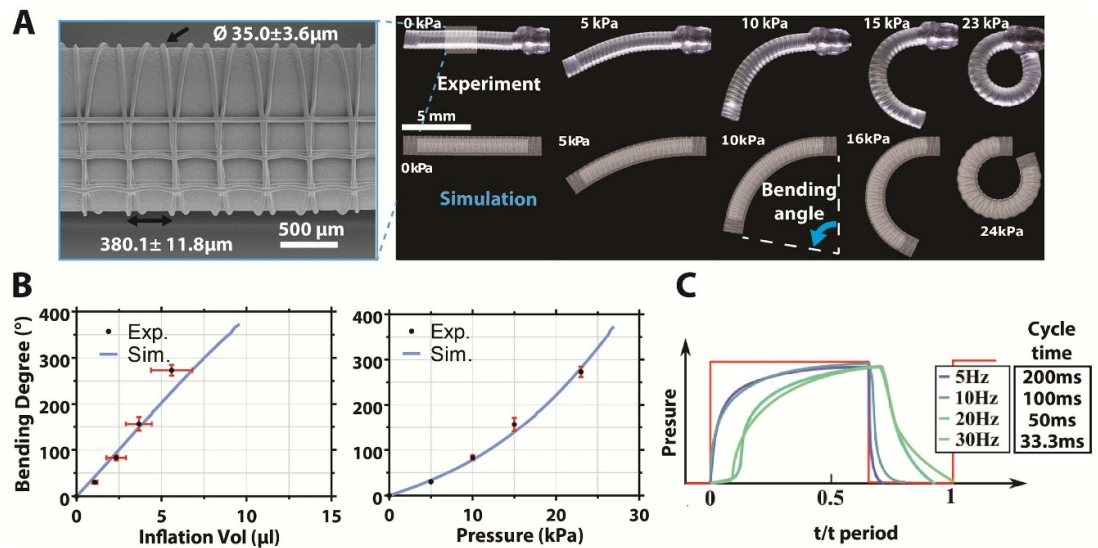


Figure 4. Characterisation of the performance of bending actuators. (A) Deformation behaviour of a representative bending actuator in comparison to the deformations obtained via simulations. Scanning electron microscopy image of the actuator is also shown. (B) Graphs of inflation volume vs deformation and input pressure vs deformation obtained via experiments ($n = 3$) and simulations. (C) Air pressure values measured while characterising the actuation performance of the bending actuators at different actuation frequencies (5, 10, 20–30 Hz). At frequencies $> \sim 10$ Hz, pressure values exceeding the regular actuation pressure requirements of the actuators were applied to be able to reach the desired pressure levels within each actuation cycle (see figure S7 for exact values). The duty cycle was kept constant (on-to-off duration ratio of 2) for all the experiments.

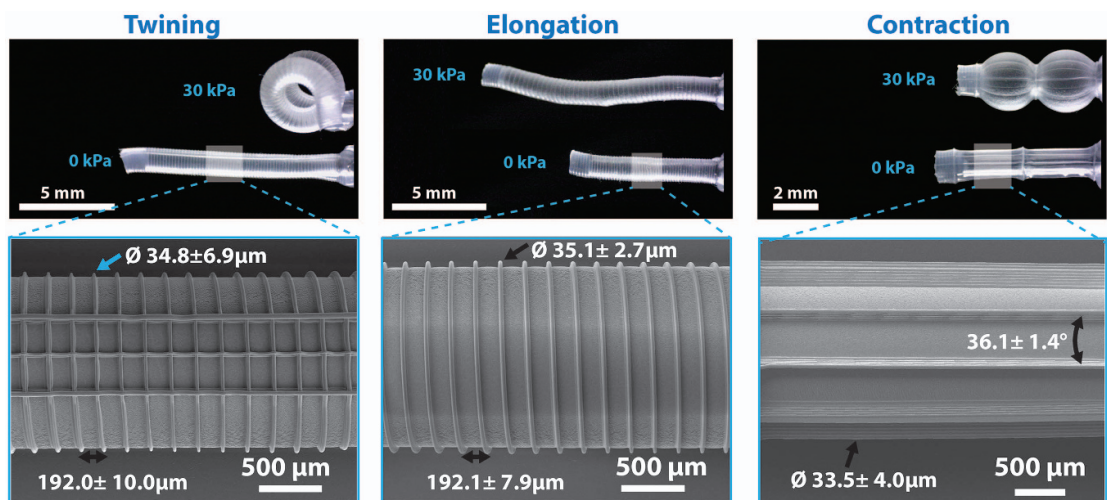
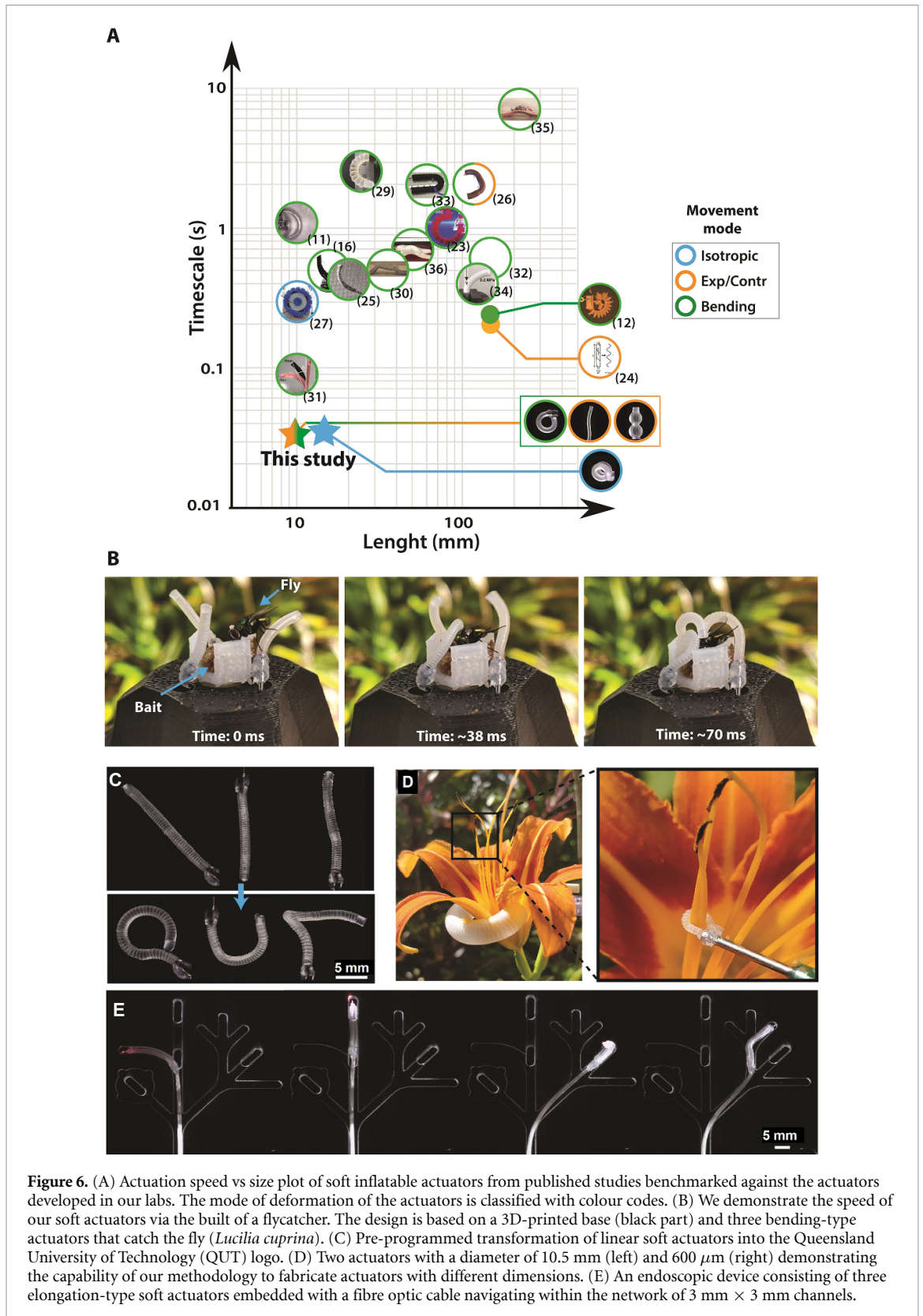


Figure 5. Miniaturised soft actuators exhibiting various movements. Representative twining-, elongation- and contraction-type actuators with their scanning electron micrographs.

deposit fibres at arbitrary positions and orientations, as displayed in figure 5. The fibre architectures that give rise to the unique deformation of these actuators are displayed using scanning electron microscope (SEM) images, where for twining we combined helical fibres with three grouped eccentric fibres, for extending we remove the eccentric fibres, and for contracting we only use eccentric fibres that are evenly spaced (see movies S3–5). Further, these actuators were dynamically tested, resulting in a maximum actuation frequency of 20 Hz for twining, 30 Hz for contraction and 30 Hz for elongation actuators (see movies S8–S10 for high-speed actuation videos, figures S2–S4 for technical drawings of the actuators and figure S6 for detailed characterisation results).

To benchmark these actuators, we have collected the dynamic data (time to complete an actuation cycle) of inflatable actuators from the literature and plotted it against their length scale (see figure 6(A)) [11, 12, 23–37]. As illustrated, research efforts towards miniaturisation have been focused on actuators with bending and extending deformations, due to a lack of advanced manufacturing techniques that are needed to create other more complex deformations [38, 39]. Actuators with other deformation modes are typically



found at larger scales [15, 40–43], where limited dynamic data is provided for them. Whereas we showed that additive manufacturing can create pathways for high dynamic actuators, typically these technologies are not well suited for miniaturisations or combining multiple materials [40, 44–49]. Therefore, as shown in figure 6(A), the majority of the miniaturised actuators were fabricated via various moulding techniques and are limited to only one actuation mode. As demonstrated, our MEW-based fabrication method provides large design flexibility, giving rise to an increase in the design space of miniaturised actuators. We identified

that our actuators are not only among the fastest in their class (actuators based on forced inflation) but also outperform their counterparts with respect to achievable deformation diversity (figure 6(A)). Our mechanical tests indicate that our bending actuators are able to exert similar contact forces when compared to a previously reported actuator design [39], yet they require approximately 5- to 10-times less air pressure. Furthermore, the collected data also points to the same conclusion as Nature-smaller systems are able to reach higher actuation speeds.

Finally, to demonstrate the performance of our actuators, we applied them in a setting where speed, small scale and compliance are of the utmost importance: catching a fly without killing it. Towards this goal, we developed a soft robotic flycatcher (figure 6(B)). The flycatcher consists of three bending actuators that are placed in a triangular pattern around a 3D-printed base with a central cylindrical target area (see supplementary text for further information and figure 9 for the technical drawing). When a fly is detected, we apply air pressure to the three bending actuators using a syringe, rapidly closing the trap, successfully catching the fly in the process (see figure 6(B) and movie S11). Furthermore, by combining various actuator designs in a linear or parallel manner, a wide range of miniaturised compliant devices such as actuators that transform into very complex shapes (figures 6(C) and (D) and movie S12) and endoscopic systems that are able to navigate through complex and constrained environments (figures 6(E) and S10 and movie S13) can be developed.

3. Conclusions

In conclusion, by enabling the seamless implementation of the concepts of fibre-reinforcement to control volumetric expansion and miniaturisation, we were able to create a wide variety of actuator deformations with the application of only a few microliters of actuation volume. As volume flux is typically the limiting factor for speed, we were able to create high dynamic motions (up to ~ 30 Hz) using standard pressure regulators. Our additive manufacturing-based automated manufacturing platform allowed us to down-scaling the dimensions of fibre-reinforced actuators without compromising their functionality. Such actuators that operate with low-volume and -pressure fluids and exhibit minor volumetric changes are also highly advantageous in applications where space of operation is limited. Arrays of these actuators may be useful in locomotion, fluid transportation, propelling and mixing, as well as complex grasping and manipulation tasks. In the present study, we focused our investigation on inflatable elastomers. Yet, in future studies, alternative actuation methods can be explored by incorporating different matrix materials that respond to alterations in osmotic conditions, pH, magnetic fields or temperatures. The deformation of this type of soft matter can be guided via our 3D-printed fibrous network, which may unlock new research directions towards the development of a new generation of soft smart materials, actuators and robots.

4. Experimental

4.1. Fabrication of soft actuators

The fabrication process of the actuators starts with the application of a viscous platinum-catalysed silicone (Ecoflex 00–10, Smooth-On Inc., USA) onto the printing collector (rod) of the MEW device. First, parts A and B of the silicon were mixed and stirred thoroughly for 2 min (1A:1B by volume), drawn into a positive displacement pipette and applied to the rotating printing collector after 18 min until a volume sufficient for a wall thickness of ~ 200 μm is deposited. With the aid of a 0.5 mm diameter metal rod attached to the print head of the MEW system that lightly touches the rotating printing collector, the partially-cured silicon was uniformly dispersed by moving the translational linear stage of the system back and forth along the main axis of the printing collector for ~ 3 min while it was rotating. Subsequently, the printing process of the fibrous network onto the partially-cured silicon was commenced (see movie S1 for the fabrication process).

For the preparation of the MEW device, first, medical-grade polycaprolactone pellets (Purasorb PC 12, Purac Biomaterials, the Netherlands) were placed in a syringe and heated to a temperature of 80 $^{\circ}\text{C}$ in the extrusion head of the device. After allowing the polymer to reach a steady molten state (~ 10 mins), air pressure of 1.5 bar was applied to the syringe using an electro-pneumatic pressure regulator (ITV0030, SMC, Japan) to extrude the molten polymer through a 23 G needle. During the extrusion, a voltage of 4.9–5 kV was applied to the needle that leads to the formation of a fine, stable polymeric jet. The printing collector-to-needle distance was set to 3 mm, and the jet was deposited onto the collector at a speed of 165 mm min^{-1} (combined translational (linear stage) and tangential speed (rotational stage)). MEW is a computer-aided manufacturing technique that utilises programs written in G-Code-based numerical controlling language (see table S2). The fibrous networks were printed onto the partially-cured silicone to enhance the adhesion between the matrix material and fibres. After the completion of the printing process, the silicone was left to fully cure for 2 h. The actuators were then peeled off the rods with ethanol aiding as a

lubricant. The actuators were mounted to a pressure source after sealing their tip with air-curing silicone (Sil-Poxy, Smooth-On Inc., USA).

4.2. Characterisation of the soft pneumatic actuators

4.2.1. SEM

The micrographs of the actuators and fibrous networks were acquired using a Tescan MIRA3 SEM. Samples were first gold-coated for 75 s at 30 mA (Leica EM-SCD005 gold sputter coater, Wetzlar, Germany) before imaging.

4.2.2. Characterization of the movement in response to pressure

The actuators were driven with air using a custom-made syringe pump, and their static images, as well as their videos, were acquired using a handheld digital microscope (Dino-Lite Edge 5MP, AnMo Electronics Corporation). The pressure values within the system were measured using a pressure sensor (HSCDANN005PGAA5, Honeywell Sensing and Productivity Solutions), which is placed next to the actuators.

4.2.3. High-frequency and rapid actuation tests (dynamic)

For the high-frequency actuation tests, a pneumatic system (Performus VII, Nordson Electron Fusion Devices, Inc) controlled by an external microcontroller was used. The pressure of the delivered air was adjusted for each actuator type to enable their full range of motion within the duration of each actuation cycle (see figure S7). At higher frequencies ($> \sim 10$ Hz), high-pressure values exceeding the regular actuation requirements of the actuators was set as the response of the system was found to be slow to reach the desired levels in the given time if high-pressure values are not used. The pressure values were measured using a pressure sensor (HSCDANN005PGAA5, Honeywell Sensing and Productivity Solutions), which was placed at the actuator-end of the experimental setup.

4.2.4. Measurement of the volumetric expansion (static)

The volumetric expansion of the actuators after their actuation was quantified by measuring the amount of fluid (H_2O) that is delivered with a positive displacement pipette. The actuators were submerged in water during the tests to avoid the deformations caused by the weight of the supplied water.

4.2.5. Simulations

The response of our actuators upon inflation was modelled using the FE method, using the commercial package ABAQUS (2019/Standard). In the fibre actuator analyses, the silicone rubber was modelled as an incompressible Neo-Hookean hyperelastic material model with an initial shear modulus μ_0 of 30 kPa. The fibres were modelled as a linear elastic material with Young's modulus E of 320 MPa and a Poisson ratio ν of 0.3. The cylindrical rubber tube was discretised using 3D tetrahedral hybrid solid elements (element code C3D10H), while the fibres were discretised using three-node quadratic beam elements (element code B32). The fibres and cylindrical tube are meshed separately and connected using a tie constraint that allows no slipping of the fibres relative to the tube. We pressurise the actuators by supplying incompressible fluid to the internal cavity while monitoring the pressure inside and simulate the quasi-static behaviour using a static solver.

Data availability statement

All data that support the findings of this study are included within the article (and any supplementary files).

Acknowledgments

The authors thank Mr Pawel Mieszczanek and Mr Aaron Foster for their assistance in the experiments. The authors acknowledge the Central Analytical Research Facility of the Institute for Future Environments at QUT. This work was financially supported by the Australian Research Council Industrial Transformation Training Centre (external ref: IC160100026, Queensland University of Technology) and by the Hans Fischer Senior Fellowship at the Institute for Advanced Study, Technische Universitaet München.

Author contributions

O B initiated and conceived the research, performed experiments, analysed data and drafted the manuscript; B G performed the simulations, contributed to the design of the study, interpretation of the data and writing

of the manuscript; S L contributed to the design, fabrication and characterisation of the soft actuators; T S performed SEM imaging; K B and D WH provided direction and edited the manuscript.

Conflict of interest

The authors declare no competing interests.

Supplementary information

The online version contains supplementary material.

ORCID iDs

Onur Bas  <https://orcid.org/0000-0001-8841-5443>

Benjamin Gorissen  <https://orcid.org/0000-0001-8275-7610>

Tara Shabab  <https://orcid.org/0000-0003-4159-7440>

Katia Bertoldi  <https://orcid.org/0000-0002-5787-4863>

Dietmar W Huttmacher  <https://orcid.org/0000-0001-5678-2134>

References

- [1] Laschi C, Mazzolai B and Cianchetti M 2016 Soft robotics: technologies and systems pushing the boundaries of robot abilities *Sci. Robot.* **3** 690 eaa3690
- [2] Ricotti L, Trimmer B, Feinberg A W, Raman R, Parker K K, Bashir R, Sitti M, Martel S, Dario P and Menciassi A 2017 Biohybrid actuators for robotics: a review of devices actuated by living cells *Sci. Robot.* **2** eaaq0495
- [3] Yang G-Z et al 2018 The grand challenges of science robotics *Sci. Robot.* **3** eaar7650
- [4] Alici G 2018 Softer is harder: what differentiates soft robotics from hard robotics? *MRS Adv.* **3** 1557–68
- [5] Gorissen B, Reynaerts D, Konishi S, Yoshida K, Kim J W and De Volder M 2017 Elastic inflatable actuators for soft robotic applications *Adv. Mater.* **29** 1–14
- [6] Gorissen B, Melancon D, Vasios N, Torbati M and Bertoldi K 2020 Inflatable soft jumper inspired by shell snapping *Sci. Robot.* **5** eabb1967
- [7] Baumgartner R et al 2020 A lesson from plants: high-speed soft robotic actuators *Adv. Sci.* **7** 1903391
- [8] Pal A, Goswami D and Martinez R V 2020 Elastic energy storage enables rapid and programmable actuation in soft machines *Adv. Funct. Mater.* **30** 1–9
- [9] Shepherd R F, Stokes A A, Freaake J, Barber J, Snyder P W, Mazzeo A D, Cademartiri L, Morin S A and Whitesides G M 2013 Using explosions to power a soft robot *Angew. Chem., Int. Ed.* **52** 2892–6
- [10] Skotheim J M and Mahadevan L 2005 Plant science: physical limits and design principles for plant and fungal movements *Science* **308** 1308–10
- [11] Gorissen B, De Volder M, De Greef A and Reynaerts D 2011 Theoretical and experimental analysis of pneumatic balloon microactuators *Sensors Actuators A* **168** 58–65
- [12] Mosadegh B, Polygerinos P, Keplinger C, Wennstedt S, Shepherd R F, Gupta U, Shim J, Bertoldi K, Walsh C J and Whitesides G M 2014 Pneumatic networks for soft robotics that actuate rapidly *Adv. Funct. Mater.* **24** 2163–70
- [13] Connolly F, Polygerinos P, Walsh C J and Bertoldi K 2015 Mechanical programming of soft actuators by varying fiber angle *Soft Robot.* **2** 26–32
- [14] Shapiro Y, Wolf A and Gabor K 2011 Bi-bellows: pneumatic bending actuator *Sens. Actuators A* **167** 484–94
- [15] Connolly F, Walsh C J and Bertoldi K 2017 Automatic design of fiber-reinforced soft actuators for trajectory matching *Proc. Natl Acad. Sci.* **114** 51–56
- [16] Galloway K C, Polygerinos P, Walsh C J and Wood R J 2013 Mechanically programmable bend radius for fiber-reinforced soft actuators *2013 16th Int. Conf. Adv. Robot. ICAR* pp 1–6
- [17] Kim S Y, Baines R, Booth J, Vasios N, Bertoldi K and Kramer-Bottiglio R 2019 Reconfigurable soft body trajectories using unidirectionally stretchable composite laminae *Nat. Commun.* **10** 3464
- [18] Cappello L, Galloway K C, Sanan S, Wagner D A, Granberry R, Engelhardt S, Haufe F L, Peisner J D and Walsh C J 2018 Exploiting textile mechanical anisotropy for fabric-based pneumatic actuators *Soft Robot.* **5** 662–74
- [19] Sinatra N R, Teeple C B, Vogt D M, Parker K K, Gruber D F and Wood R J 2019 Ultragentle manipulation of delicate structures using a soft robotic gripper *Sci. Robot.* **4** eaax5425
- [20] Sinatra N R, Ranzani T, Vlassak J J, Parker K K and Wood R J 2018 Nanofiber-reinforced soft fluidic micro-actuators *J. Micromech. Microeng.* **28** 084002
- [21] Brown T D, Dalton P D and Huttmacher D W 2011 Direct writing by way of melt electrospinning *Adv. Mater.* **23** 5651–7
- [22] Wunner F M, Wille M-L, Noonan T G, Bas O, Dalton P D, De-Juan-Pardo E M and Huttmacher D W 2018 Melt electrospinning writing of highly ordered large volume scaffold architectures *Adv. Mater.* **30** 1706570
- [23] Gorissen B, De Volder M and Reynaerts D 2015 Pneumatically-actuated artificial cilia array for biomimetic fluid propulsion *Lab Chip* **15** 4348–55
- [24] Marchese A D, Katzschmann R K and Rus D 2015 A recipe for soft fluidic elastomer robots *Soft Robot.* **2** 7–25
- [25] Sasaki D, Noritsugu T and Takaiwa M 2005 Development of active support splint driven by pneumatic soft actuator (ASSIST) *Proc.-IEEE Int. Conf. Robot. Autom.* pp 520–5
- [26] Kato N, Ando Y, Tomokazu A, Suzuki H, Suzumori K, Kanda T and Endo S 2008 *Elastic Pectoral Fin Actuators for Biomimetic Underwater Vehicles BT—Bio-mechanisms of Swimming and Flying* ed N Kato and S Kamimura (Tokyo: Springer) pp 271–82
- [27] Tolley M T, Shepherd R F, Mosadegh B, Galloway K C, Wehner M, Karpelson M, Wood R J and Whitesides G M 2014 A resilient, untethered soft robot *Soft Robot.* **1** 213–23

- [28] Shepherd R F, Ilievski F, Choi W, Morin S A, Stokes A A, Mazzeo A D, Chen X, Wang M and Whitesides G M 2011 Multigait soft robot *Proc. Natl Acad. Sci. USA* **108** 20400–3
- [29] Konishi S, Kawai F and Cusin P 2001 Thin flexible end-effector using pneumatic balloon actuator *Sens. Actuators A* **89** 28–35
- [30] Yuk H, Lin S, Ma C, Takaffoli M, Fang N X and Zhao X 2017 Hydraulic hydrogel actuators and robots optically and sonically camouflaged in water *Nat. Commun.* **8** 14230
- [31] Chou C P and Hannaford B 1996 Measurement and modeling of McKibben pneumatic artificial muscles *IEEE Trans. Robot. Autom.* **12** 90–102
- [32] Suzumori K, Iikura S and Tanaka H 1991 Development of flexible microactuator and its applications to robotic mechanisms *Proc.-IEEE Int. Conf. Robotics and Automation* vol 2 pp 1622–7
- [33] Polygerinos P, Wang Z, Galloway K C, Wood R J and Walsh C J 2015 Soft robotic glove for combined assistance and at-home rehabilitation *Robot. Autom. Syst.* **73** 135–43
- [34] Gong X, Yang K, Xie J, Wang Y, Kulkarni P, Hobbs A S and Mazzeo A D 2016 Rotary actuators based on pneumatically driven elastomeric structures *Adv. Mater.* **28** 7533–8
- [35] Takemura K, Yokota S and Edamura K 2005 A micro artificial muscle actuator using electro-conjugate fluid *Proc.-IEEE Int. Conf. Robot. Autom.* pp 532–7
- [36] Yamaguchi A, Takemura K, Yokota S and Edamura K 2011 A robot hand using electro-conjugate fluid *Proc.-IEEE Int. Conf. Robot. Autom.* pp 5923–8
- [37] Correll N, Önal Ç D, Liang H, Schoenfeld E and Rus D 2014 Soft autonomous materials—using active elasticity and embedded distributed computation BT—experimental robotics *The 12th Int. Symp. Experimental Robotics* ed O Khatib, V Kumar and G Sukhatme (Berlin: Springer) pp 227–40
- [38] Hines L, Petersen K, Lum G Z and Sitti M 2017 Soft actuators for small-scale robotics *Adv. Mater.* **29** 1603483
- [39] Udupa G, Sreedharan P, Dinesh P S and Kim D 2014 Asymmetric bellow flexible pneumatic actuator for miniature robotic soft gripper *J. Robot.* **2014** 902625
- [40] Schaffner M, Faber J A, Pianegonda L, Rühs P A, Coulter F and Studart A R 2018 3D printing of robotic soft actuators with programmable bioinspired architectures *Nat. Commun.* **9** 878
- [41] Singh G and Krishnan G 2020 Designing fiber-reinforced soft actuators for planar curvilinear shape matching *Soft Robot.* **7** 109–21
- [42] Buckner T L and Kramer-Bottiglio R 2018 Functional fibers for robotic fabrics *Multifunct. Mater.* **1** 012001
- [43] Deimel R and Brock O 2013 A compliant hand based on a novel pneumatic actuator *Proc.-IEEE Int. Conf. Robot. Autom.* pp 2047–53
- [44] Maccurdy R, Katzschmann R, Kim Y and Rus D 2016 Printable hydraulics: a method for fabricating robots by 3D co-printing solids and liquids *Proc.-IEEE Int. Conf. Robot. Autom. (June 2016)* pp 3878–85
- [45] Peele B N, Wallin T J, Zhao H and Shepherd R F 2015 3D printing antagonistic systems of artificial muscle using projection stereolithography *Bioinspir. Biomim.* **10** 055003
- [46] Zolfagharian A, Kouzani A Z, Yang S, Ali A, Moghadam A, Gibson I and Kaynak A 2016 Sensors and actuators A: physical evolution of 3D printed soft actuators *Sens. Actuators A* **250** 258–72
- [47] Tawk C, Panhuis M, Spinks G M and Alici G 2018 Bioinspired 3D printable soft vacuum actuators *Soft Robot.* **5** 685–94
- [48] Wallin T J, Pikul J and Shepherd R F 2018 3D printing of soft robotic systems *Nat. Rev. Mater.* **3** 84–100
- [49] Skylar-Scott M A, Mueller J, Visser C W and Lewis J A 2019 Voxellated soft matter via multimaterial multinozzle 3D printing *Nature* **575** 330–5

Supporting Information

Ultrafast, Miniature Soft Actuators

Onur Bas^{1,2}, Benjamin Gorissen³, Simon Luposchinsky^{2,4}, Tara Shabab², Katia Bertoldi³, Dietmar W. Hutmacher^{1,2*}*

¹ ARC Industrial Transformation Training Centre in Additive Biomanufacturing, Queensland University of Technology (QUT), Brisbane, QLD 4059, Australia.

² School of Mechanical, Medical and Process Engineering, Queensland University of Technology (QUT), Brisbane, QLD 4001, Australia.

³ Harvard John A. Paulson School of Engineering and Applied Sciences, Harvard University, Cambridge, MA 02138, USA.

⁴ Department of Functional Materials in Medicine and Dentistry, University of Würzburg, Pleicherwall 2, Würzburg, 97070, Germany.

Corresponding authors: o.bas@qut.edu.au , dietmar.hutmacher@qut.edu.au

Characterisation of printing accuracy

The deposition accuracy of the fibres, as well as the wall thickness of the silicon body of the actuators, were evaluated using an image processing software ImageJ (National Institutes of Health, USA) on scanning electron microscopy micrographs. The distance between the helical fibres (pitch size) of bending, twinning and elongation-type actuators was measured. Arc angle between the longitudinal places fibres of contraction type (from cross-section views) was measured.

Mechanical characterisation of the soft actuators

The performance (bending, pulling, holding, pushing, contraction force) of the actuators were characterised using Instron MicroTester (Instron, Australia) equipped with 5N load cell. The displacement rate of 1mm/sec was applied holding force of bending and twinning actuators.

Design and development of the flycatcher

For the fabrication of the flycatcher, three bending-type actuators were placed in a triangular pattern around a 3D-printed base (Polylactic acid) (see **Figure S9** for the technical drawing of the flycatcher). All the actuators were connected to a single syringe via tubing and activated all together by pushing the piston of a syringe. We used meat to attract a fly to the centre of the flycatcher.

Finite element analyses

The responses of all actuators upon inflation was modelled using the Finite Element (FE) method, using the commercial package ABAQUS (2019/Standard). Three different type of simulations were run throughout the research:

- The eccentric void actuators (see **Figure 1**), was discretized using second-order hybrid tetrahedral elements (C3D10H). The material was modelled as an incompressible Arruda-Boyce rubber with an initial shear modulus of 30 kPa and a locking stretch λ_m of 3.9. Geometrical parameters were taken from [Ref 11]
- The corrugated membrane actuators (see **Figure 1**) consist of an elastomeric part that is bonded to a layer of paper. Geometrical and material parameters were taken from [Ref 12]. The elastomer discretized using second-order hybrid tetrahedral elements (C3D10H), the paper using triangular thin shell elements (STRI65).
- All fibre-reinforced actuators in the manuscripts consist out of an elastomeric tube surrounding by strain-limiting fibres. we have discretised the cylinder using second-order hybrid tetrahedral elements (C3D10H), while the fibres were discretised using 3-node quadratic beam elements (B32). We modelled the material of the cylinder as neo-Hookean, while the fibres are assumed to be linear elastic with a Poisson's ratio of 0.3. Regarding the fibre-reinforced actuator of **Figure 1**, the geometrical and material parameters were taken from [Ref 13]. Regarding the fibre-reinforced actuators of **Figure 2**, we have used the geometrical parameters as depicted in Figure S1, and varied the material parameters between $7.5\text{kPa} < \mu_0 < 120\text{kPa}$ for the matrix and $80\text{Mpa} < E < 1.28\text{Gpa}$ for the fibres.

Writing QUT logo

To show the versatility of our fabrication process, and the fact that fibre arrangements do not have to be constant over the actuator length, we designed three linear actuators that transform into the shape of “QUT” (the acronym of the Queensland University of Technology) when actuated (**Movie S12**). By segmenting the letters into zones of constant deformation, we can convert the intricate shapes into an axial combination of archetypical deformations. We

designed each segment independently to reach its final deformation at a certain pressure that is fixed along all connected segments. This is done using finite element modelling where a scripted program is used to a cycle of different fibre arrangements. The resulting fibre arrangement is then axially stitched together and printed using our MEW process. When pressurizing the three actuators, we indeed see the three letters (QUT) emerging.

Endoscopic device

By axially combining three elongating actuators into a monolithic structure, we end up with a 3 DOF (2DOF bending + extension) soft robot that is able to navigate through complex and constrained environments (**Figure S10** and **Movie S13**). While the general motion of this robot is determined by a global pushing movement, the actuators are used for steering. As our production process is compatible with medical-grade rubbers and fibre materials, we can envision using this robot for catheterisations and other minimally invasive operations. **Movie S13** show the experimental validation of this system in a 3D constrained environment. By selectively inflating one, two or all supply channels in coordination, we can steer the robot throughout a mock-up setup, and reach all the different branches rapidly.

This endoscopic device was assembled by glueing three miniaturised version (inner diameter 800 μm instead of 1 mm) of the elongation-type soft actuators described in the previous sections using a silicone rubber (Sil-Poxy™, Smooth-On Inc., USA). A fibre optic cable was placed at the centre of these actuators. Each actuator in the assembly was connected to a separate microtubing and independently activated using a syringe. For the development of the mock setup, several layers of acrylic sheets were laser-cut and glued together to attain network of 3 mm x 3 mm square channels.

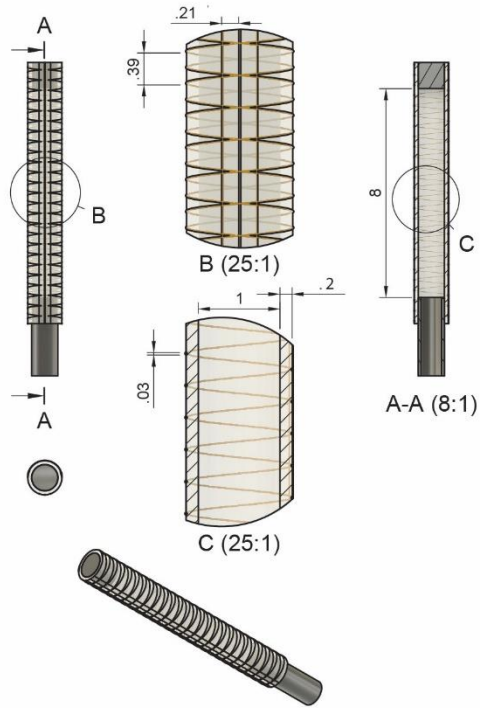


Figure S1. Technical drawing of bending actuators (units mm).

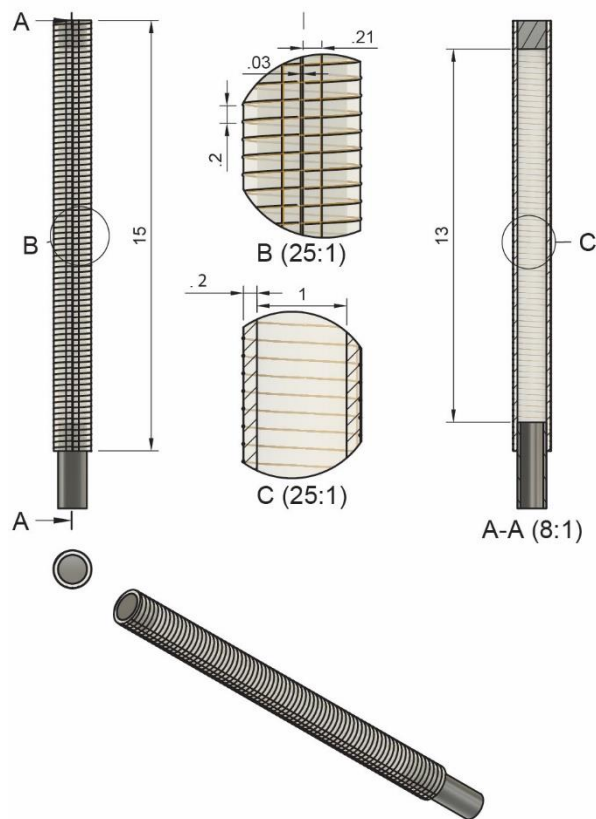


Figure S2. Technical drawing of twining actuators (units mm).

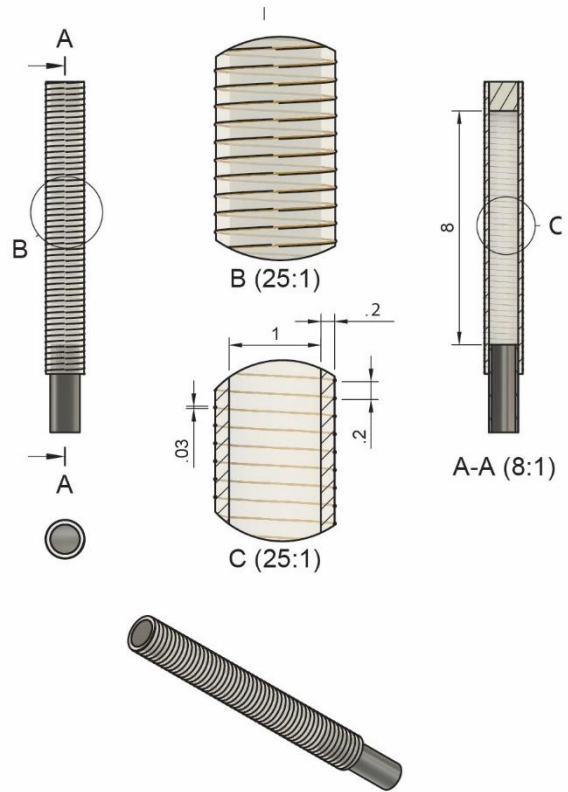


Figure S3. Technical drawing of elongation actuators (units mm).

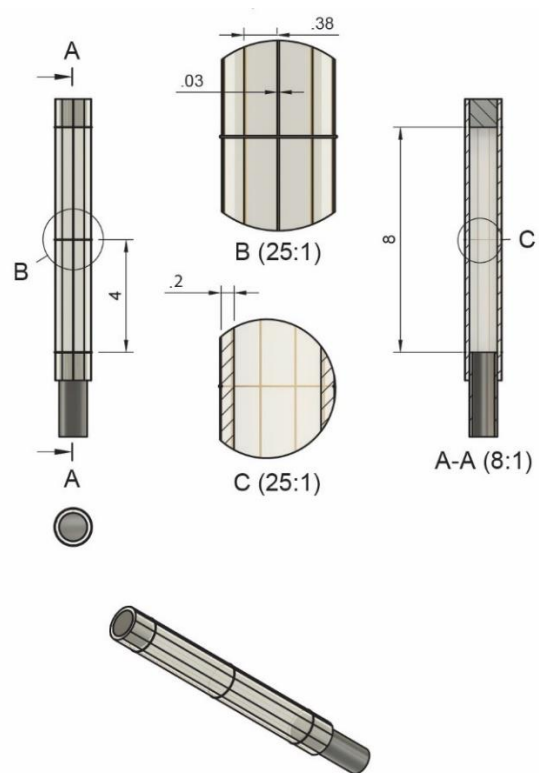


Figure S4. Technical drawing of contraction actuators (units mm).



Figure S5. Bending actuator without helical fibres exhibiting large parasitic deformations

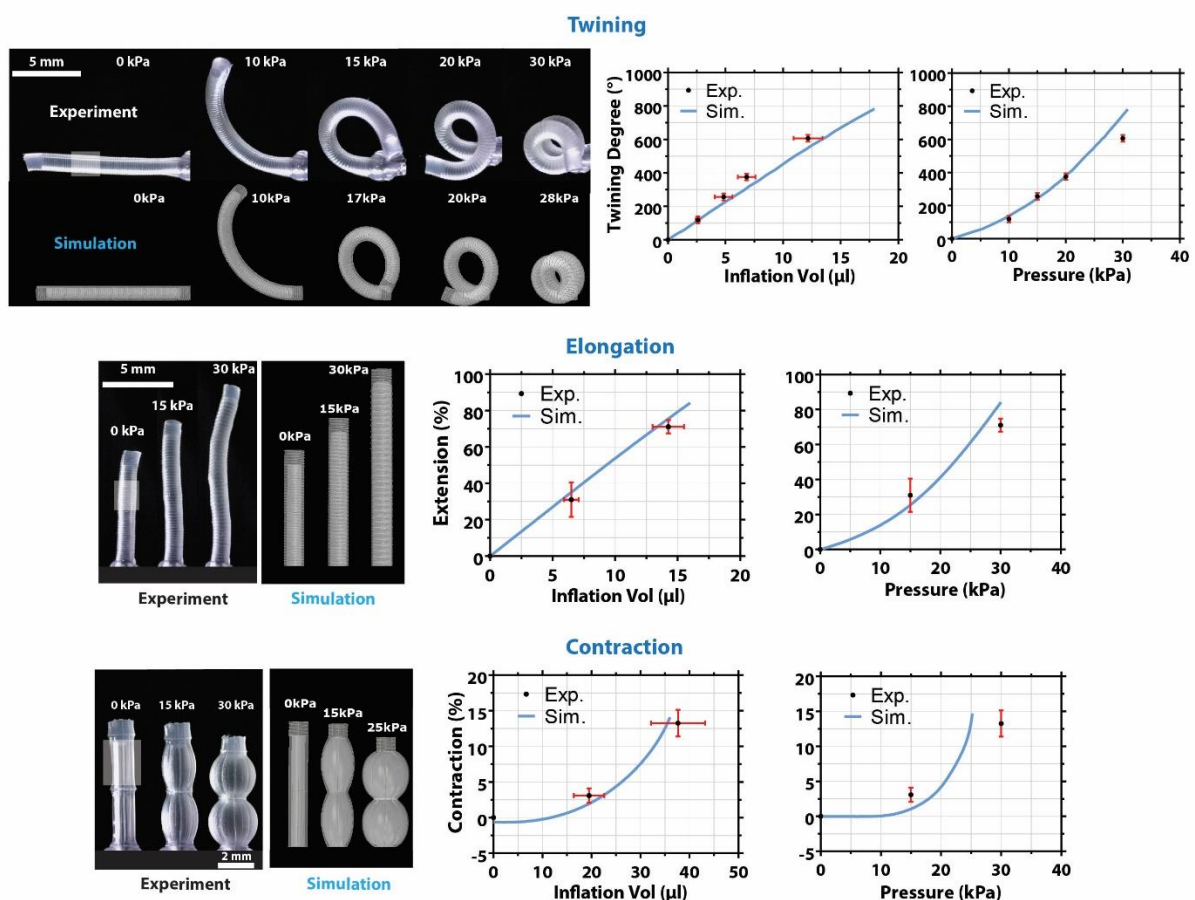


Figure S6. Deformation behaviour and actuation performance of various composite soft actuators. (A-D) Representative twining-, elongation- and contraction-type actuators with their scanning electron microscopy images as well as their simulated deformation behaviour. Graphs of inflation volume vs deformation and input pressure vs deformation obtained via experiments (n=3) and simulations are also shown.

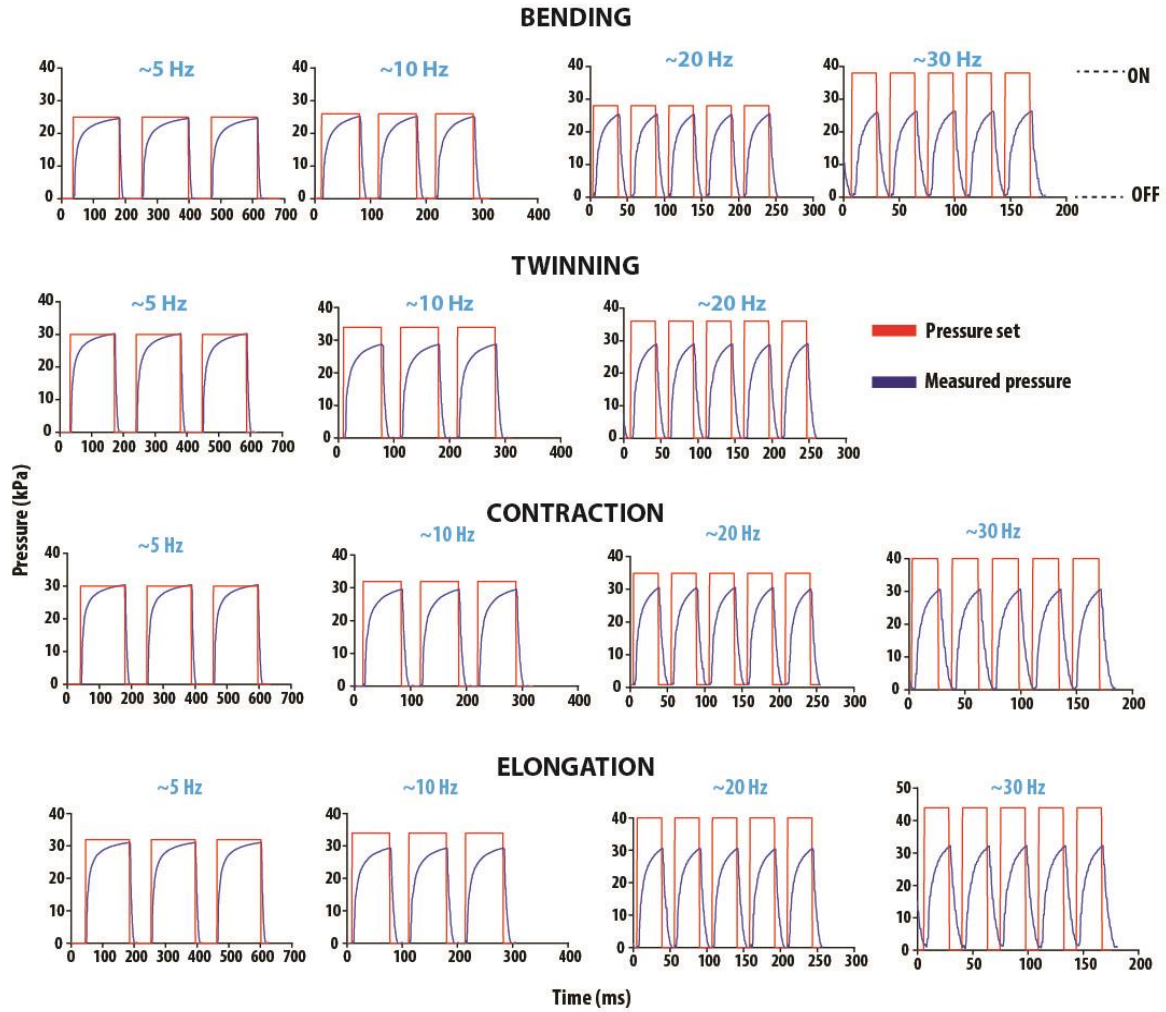


Figure S7. Air pressure values measured while characterising the actuation performance of the actuators at different actuation frequencies (5, 10, 20 to 30 Hz). At frequencies $> \sim 10$ Hz, pressure values exceeding the regular actuation pressure requirements of the actuators were applied to be able to reach the desired pressure levels within each actuation cycle. The duty cycle was kept constant (on-to-off duration ratio of 2) for all the experiments.

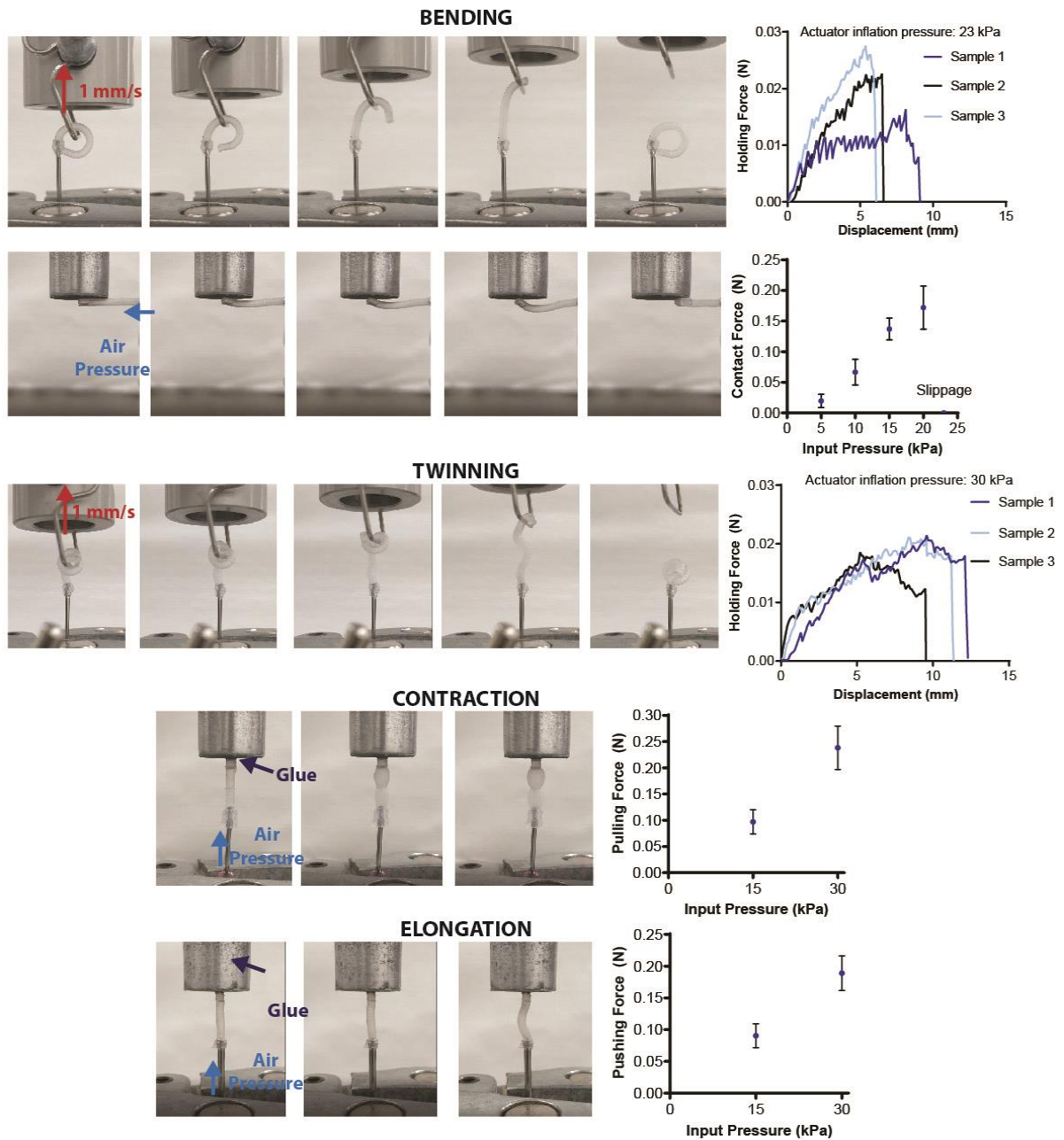


Figure S8. Two bending-type soft actuators with a diameter of (A) 600µm and (B) 10.5mm.

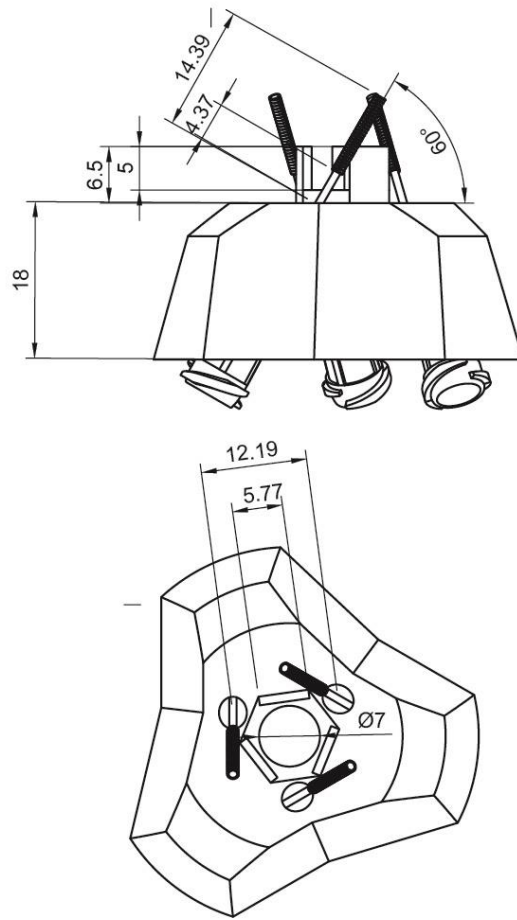


Figure S9. Technical drawing of the flycatcher.

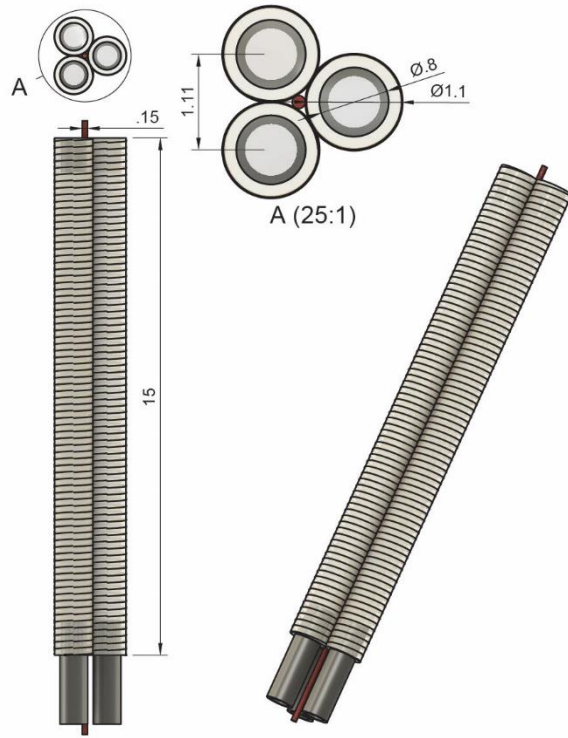


Figure S10. Technical drawing of the endoscopic device.

Table S1. Characterisation of the fabricated soft actuators

<i>Actuator Type</i>	<i>Fibre Distance (helical fibres) (μm)</i>		<i>Silicone Wall Thickness (μm)</i>	
	<i>Target</i>	<i>Fabricated (n=10)</i>	<i>Target</i>	<i>Fabricated (n=6)</i>
<i>Bending</i>	390	380.12 \pm 11.78	200	206.57 \pm 4.28
<i>Twinning</i>	200	192.05 \pm 10.04	200	187.62 \pm 7.88
<i>Elongation</i>	200	192.13 \pm 7.91	200	212.27 \pm 4.72
	<i>Arc angle (longitudinal fibres) ($^{\circ}$)</i>		<i>Silicone Wall Thickness (μm)</i>	
	<i>Target</i>	<i>Fabricated (n=10)</i>	<i>Target</i>	<i>Fabricated (n=6)</i>
<i>Contraction</i>	36	36.08 \pm 1.41	200	210.57 \pm 6.53

Table S2. GCodes used for the additive manufacturing of the actuators

OPERATIONS	ARCHETYPICAL ACTUATORS			
	BENDING	TWINING	ELONGATION	CONTRACTION
INITIALISATION	G18 G91	G18 G91	G18 G91	G18 G91
SILICONE SPREADING	F375 G1 Y31 X15 M98 P1250 L5 G92 Z0 G1 Y-5	F375 G1 Y31 X15 M98 P1250 L5 G92 Z0 G1 Y-5	F375 G1 Y31 X15 M98 P1250 L5 G92 Z0 G1 Y-5	F375 G1 Y31 X15 M98 P1250 L5 G1 Y-5
RETURN TO PRINT SETUP	G90 G1 X0 Y0 F165 G91	G90 G1 X0 Y0 F165 G91	G90 G1 X0 Y0 F165 G91 G92 Z0	G90 G1 X0 Y0 F165 G91
PRINTING THE FIBROUS NETWORKS	M98 P1266 L3 G90 G1 X0 M30	M98 P1266 L3 G90 G1 X0 M30	M98 P1266 L3 G1 Y15 G90 G1 X0 G91 M30	G1 X15 Z240 G92 Z0 M98 P1266 L6 G90 G1 X0 M30
FIBRE PRINT LOOP SUB-PROGRAM	O1266 G90 F165 G1 X-5 Z50 G1 X0 Z0 G1 X75 Z600	O1266 G1 X65 Z1040 G1 X1 F500 G1 X6 Z-1040 F165 G90	O1266 G1 X65 Z1040 G1 Y20 F500 G1 X-65 Z-1040 F165	O1266 G1 X50 G1 Z0.3142 G1 X-50 G1 Z0.3142 G1 X50 G1 Z0.3142

	G1 Y23 G1 Z650 G1 X0 G1 Y0 G1 Z600 G1 X-5 Z650 G1 X0 Z600 G1 X75 Z0 G1 Z0.5 G1 X1 G1 X0 G1 Z0.7 G1 X75 G1 Z0.3 G1 X0 G1 Z0 F165 G91 M99	G1 X15 G92 Z0 G1 Z 0.2 G1 X66 G1 Z-0.2 G1 X0 G1 Z0 G91 M99	G1 Y-20 G1 X-2 G1 X2 M99	G1 X-50 G1 Z0.3142 G1 X50 G1 Z0.3142 G1 X-50 G1 Z0.3142 G1 X50 G1 Z0.3142 G1 X-50 G1 Z0.3142 G1 X50 G1 Z0.3142 G1 X-1.5 G1 X-1.5 Z- 25.136 G1 Z-12.568 G1 X-4 G4 P0.5 G1 Z12.568 G1 X-4 G4 P0.5 G1 Z-12.568 G1 X-1.5 Z- 25.136 G1 X-1 G1 X-1.5 Z- 25.136 G1 Z-12.568 G1 X-4 G4 P0.5 G1 Z12.568 G1 X-4 G4 P0.5 G1 Z-12.568 G1 X-1.5 Z- 25.136 G1 X-1 G1 X-1.5 Z- 25.136 G1 Z-12.568 G1 X-4 G4 P0.5 G1 Z12.568 G1 X-4
--	---	--	-----------------------------------	--

				G4 P0.5 G1 Z-12.568 G1 X-1.5 Z-25.136 G1 X-1 G1 X-1.5 Z-25.136 G1 Z-12.568 G1 X-4 G4 P0.5 G1 Z12.568 G1 X-4 G4 P0.5 G1 Z-12.568 G1 X-1.5 Z-25.136 G1 X-1.5 G90 G1 X0 Z0 G1 X15 G91 M99
SILICONE SPREADING LOOP SUB-PROGRAM	O1250 G1 X50 Z-100 G1 X-50 Z-100 M99			